Hindawi
Shock and Vibration
Volume 2017, Article ID 9760940, 11 pages
https://doi.org/10.1155/2017/9760940

Research Article

Acoustic Emission Monitoring and Failure Precursors of Sandstone Samples under Various Loading and Unloading Paths

Jie Xu,[1] Jingdong Jiang,[2] Lingling Zuo,[3] and Yufeng Gao[1]

[1] *Geotechnical Research Institute, Hohai University, Nanjing 210098, China*
[2] *Nanjing Hydraulic Research Institute, Nanjing 210029, China*
[3] *Laixi Water Conservancy Bureau, Laixi 266600, China*

Correspondence should be addressed to Jingdong Jiang; 365354266@qq.com

Received 21 July 2017; Accepted 17 October 2017; Published 27 December 2017

Academic Editor: Rafał Burdzik

To explore the failure precursors of hard rock, a series of triaxial loading and unloading experiments were carried out on sandstone sample using the acoustic emission systems. The extreme-point symmetric mode decomposition method (ESMD method) was used to denoise and reconstruct the AE data. The AE quiet period in Scheme I becomes much more obvious with the confining pressure increasing, which can be regarded as the precursor information of the sample failure under conventional triaxial compression. Unlike Scheme I, there are no obvious precursory characteristics before failure in Schemes II and III, and the count rate reaches the maximum at the peak point. When the stress ratio ranges from 0.8 to 1.0, the fractal values of acoustic emission can be used to investigate the failure precursors of samples at a lower confining pressure. When the time ratio is greater than 0.8 under higher confining pressures, the fractal values of sandstone samples under unloading paths are rapidly reduced, which can be used to predict rock failure at higher confining pressures.

1. Introduction

The rock material properties, various stress paths, and wall rock conditions are complex and diverse, severely restricting the study on failure precursors of rock materials. The deformation and failure behavior of rock are the process of the inner micro cracks initiation, propagation, and coalescence [1–5]. During this process, the strain energy is continuously released in the form of the elastic wave, which is referred to as the acoustic emission (AE). It is helpful to investigate the failure mechanism of rock materials to study the AE characteristics during the failure process and the relationship between the AE parameters and rock fracture [6–11].

Chmel and Shcherbakov [12] carried out experimental study on the AE characteristics of compression and dynamic fracture in granite, which contributes to assessing the relationship between events occurring under nonequilibrium conditions. Based on the biaxial compression tests, Baddari et al. [13] adopted electromagnetic radiation and acoustic emission to study the failure process of large rock samples, and the results can provide an analysis platform for forecasting the dynamic disaster. Three triaxial compression tests on granite samples were carried out by Thompson et al. [14], and new observations of fracture nucleation were proposed according to AE monitoring. The results showed that the fracture nucleation in intact rock and the nucleation of dynamic instabilities in stick slip tests had similarity. The strength variation and AE features of skarn were investigated by Xu et al. [15] through uniaxial cyclic loading and unloading tests. The results showed that there is an apparent relative quiet stage of AE signals before failure. Zhang et al. [16] performed the uniaxial loading to research the AE characteristics of rock failure process, and the AE parameters such as cumulative AE events, AE energy release rate, and the b-value were used to investigate the precursory information of rock failure.

Existing AE studies are mainly concentrated on the relationship between stress or strain and AE parameters under a single stress path condition such as compression, tension, and shear. By contrast, there are fewer studies on the theoretical research of AE activity under a complex stress path.

Figure 1: Standard cylindrical sandstone samples used in this study.

In our paper, a series of triaxial loading and unloading experiments on sandstone samples were carried out under different stress conditions. The extreme-point symmetric mode decomposition method (ESMD method) was used to denoise and reconstruct the AE data, and the AE characteristics of sandstone samples under different stress paths were investigated. Based on the fractal theory, the influence of unloading paths on AE characteristics was quantified, which could be used to explore the failure precursors of rock and provide a theoretical basis for assessing and preventing the stress-induced stability of hard rock.

2. Test Method and Sample Preparation

2.1. Sample Preparation. The sandstone used in our study was collected from the Huainan coal mine in Anhui province, China. The results of X-ray diffraction (XRD) show that the minerals of this sandstone are 12.1% quartz, 10.9% K-feldspar, 38.7% plagioclase, 13.4% calcite, 12.7% dolomite, 2.8% hematite, and 9.4% clay minerals. The connected porosity and bulk density of the sandstone are 7.02% and 2613 kg/m^3, respectively. All sandstone samples were cored from the same block of material to an actual diameter of 50 mm and length of 100 mm, as shown in Figure 1. The permissible error of end flatness is ±0.05 mm, the diameter error is less than 0.3 mm, and the maximum deviation between the end face and axial line is not more than 0.25°. The machining precisions of all samples are in accordance with the demand of technical specifications.

2.2. Testing Equipment and Procedure. All experiments were conducted using an MTS 815 servo-controlled rock mechanics experimental system. The integral rigidity of the experiment framework is 11.0×10^9 N/m, the maximum axial force is 4600 KN, the maximum lateral pressure is 140 MPa, and the sensitivity of servo valve is 290 Hz. The whole experimental process is controlled by a computer, allowing for automatic data acquisition and processing. Acoustic emissions were monitored with a 16-channel PCI-II system. The resonant frequency and operating frequency range were 500 kHz and 200~750 kHz, respectively, and the amplification of the preamplifier and threshold were set at 55 dB to improve signal to noise ratio. The sampling frequency and the sampling length were fixed at 500 kHZ and 8192, respectively. To ensure three-dimensional position precision, 6 sensors were fixed on the outside of the triaxial pressure cell as a sensor matrix. The type of the sensors was Nano30, of which the operating frequency is 100–400 kHz. The sensors were coated with Vaseline, a coupling agent, and fixed on the surface of the samples by plastic tapes. To ensure the coupling effect of the AE sensor with the sample, a pencil lead break (PLB) should be performed before the tests began (Figure 2).

The detailed testing schemes under different stress paths are shown as follows.

(1) Conventional Triaxial Loading Tests (Scheme I). The conventional triaxial tests were conducted under different confining pressures of 10, 20, 40, and 50 MPa. First, the confining pressure was loaded to the design value at a constant rate of 0.1 MPa/s, and the samples were put into a state of uniform hydrostatic stress. Second, the confining pressure remained unchanged, and the axial stress was loaded to the sandstone samples at a constant axial displacement rate of 0.001 mm/s until failure, ensuring that complete stress-strain curves would be obtained. The peak strength obtained through conventional triaxial tests can provide a basis for the determination of the unloading point in the unloading confining pressure tests.

(2) Increasing Axial Pressure and Confining Pressure Unloading Tests (Scheme II). First, the confining pressure was loaded to the design value (10, 20, 40, and 50 MPa). Second, the confining pressure remained unchanged, and the axial stress was loaded to 80% of the peak strength obtained from conventional triaxial tests. Then, the axial stress was loaded at a constant rate of 0.3 MPa/s, and the confining pressure was simultaneously unloaded at a constant rate of 0.5 MPa/s until failure.

(3) Constant Axial Pressure and Confining Pressure Unloading Tests (Scheme III). First, the confining pressure was loaded to the design value (10, 20, 40, and 50 MPa). Second, the confining pressure remained unchanged, and the axial stress was loaded to 80% of the peak strength obtained from conventional triaxial tests. Then, the axial stress remained unchanged, and the confining pressure was simultaneously unloaded at a constant rate of 0.5 MPa/s until failure.

3. Extreme-Point Symmetric Mode Decomposition Method (ESMD Method)

3.1. Method Introduction. The background noise inevitably mixes into the AE signals during data acquisition process. Even if the experiments are carried out in the relatively sealed laboratory, the servo valve adjustment also generates mechanical noise. The noise signals can interfere in the analysis of experimental data; thus the noise-suppressed processing of AE signals is the precondition of accurate quantitative analysis of rock failure process. In this study, the ESMD method was used to denoise and reconstruct the AE data.

The EMSD method is proposed to improve the Hilbert-Huang Transform (HHT) based on four prospects: (1) The sifting process is performed by means of several inner interpolating curves, which divides these methods into ESMD I, ESMD II, ESMD III, and so on; (2) the last residual

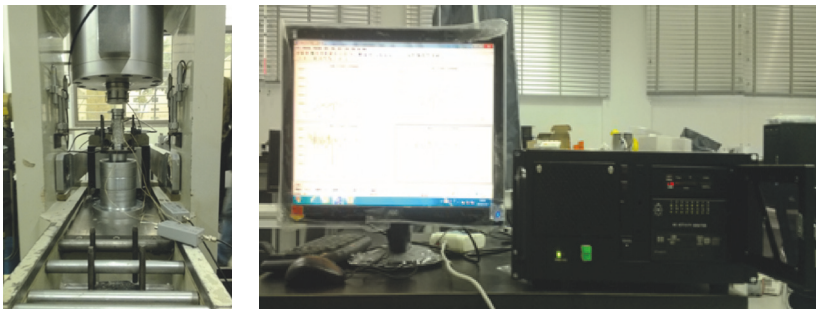

(a) Sandstone samples with AE sensors

(b) AE PCI-II

Figure 2: Sandstone samples in MTS 815 servo-controlled rock mechanics experimental system and AE PCI-II system.

is defined as an optimal curve possessing a certain number of extreme points, instead of general trend with at most one extreme point, which allows the optimal sifting times and decomposition; (3) the extreme-point symmetry is applied instead of the envelop symmetry; (4) the data-based direct interpolating approach is developed to compute the instantaneous frequency and amplitude. One advantage of the ESMD method is to determine an optimal global mean curve in an adaptive way which is better than the common least-square method and running-mean approach; another one is to determine the instantaneous frequency and amplitude in a direct way which is better than the Hilbert-spectrum method. These will improve the adaptive analysis of the data from many fields [17].

3.2. Denoising Process of AE Signals. The data decomposition of AE signals based on the ESMD can be carried out in three steps: (1) the data file named Variance_II.sce was defined according to the data file regulations, and then AE signals such as data volume and time interval were input to this data file; (2) the file established in the first step operated through the Scilab platform, which uses the least-square method to optimize the residual mode, gives the optimum screening frequency of data, and determines the optimal global mean curve in an adaptive way; (3) the self-developed file (ESMD_II.sce) operated, which can not only give the number of extreme points, but also acquire abundant information of AE data, including the trend chart, energy diagram, and spectrogram.

4. AE Characteristics of Sandstone Samples under Different Stress Paths

4.1. AE Characteristics of Samples under Loading Conditions. Figure 3 gives the curves of axial stress difference and ringing count rate with time during sandstone failure process under various confining pressures in Scheme I. At the early loading stage, the AE activity is relatively active, which comes from the closure of the initial fissure and holes. When entering into the plastic stage, the ringing count rate gradually increases, indicating that the new cracks begin to initiate in the samples. The volume expansion of samples due to the dilatation effect appears upon reaching the expansion stress, and the AE signals are enhanced significantly. When the relatively large crack occurs inside the sample, the tips of the cracks generate the stress redistribution, which accompanies the energy dissipation. During this process, the energy release rate gradually slows down, and the AE parameters such as the ringing count rate decrease, that is, the AE quiet period. As shown in Table 1 and Figure 3, the AE quiet period becomes much more obvious with the confining pressure increasing, because the amount of new cracks is relatively less due to the restriction of higher confining pressure. The time of quiet period lasts from 20 s to 57 s with the confining pressure increasing from 10 MPa to 50 MPa, and the crack propagation process transits from generation oriented to coalescence oriented small cracks.

The stress and AE characteristics of sandstone samples during the deformation process under various confining pressures are shown in the following aspects: (1) the shear failure is the main failure mode of the samples under the conventional triaxial compression, which have the higher residual strengths; (2) the stress drops after the peak becomes less distinct with the confining pressure increasing, and the residual strengths gradually increase, which comes from the more obvious restraining effect of high confining pressure to the samples; (3) the AE signals almost exist during the whole process, which as a whole are stronger; (4) with the confining pressure increasing, the ringing count rate at the peak rises from 59 times per second to 145 times per second, indicating that the sandstone samples accumulated more energy before failure and released more energy at failure due to higher confining pressure; (5) the maximum ringing count rate appears after peak instead of peak positions, which also rises with the confining pressure increasing. The reason is that the samples have larger load bearing capacity at peak positions due to the confining pressure constraints, and the obvious friction slip of broken blocks takes place only when the stress falls to the residual stress. This is consistent with the characteristics of crack propagation and coalescence during the process of rock breaking simulated by [18].

The quiet period can be regarded as the precursor information of the sample failure under conventional triaxial compression. The confining pressure changes the stress state

Table 1: Count rate of sandstone sample under various confining pressures in Scheme I.

Scheme I	Confining pressure/MPa	Axial stress difference at the peak/MPa	Time at the peak/s	Count rate at the peak/(times/s)	Time of quiet period/s	Maximum count rate/(times/s)
	10	118.1	78.3	59	20	96
	20	154.1	93.4	100	22	140
	40	199.9	134.2	118	33	134
	50	210.60	184.0	145	57	169

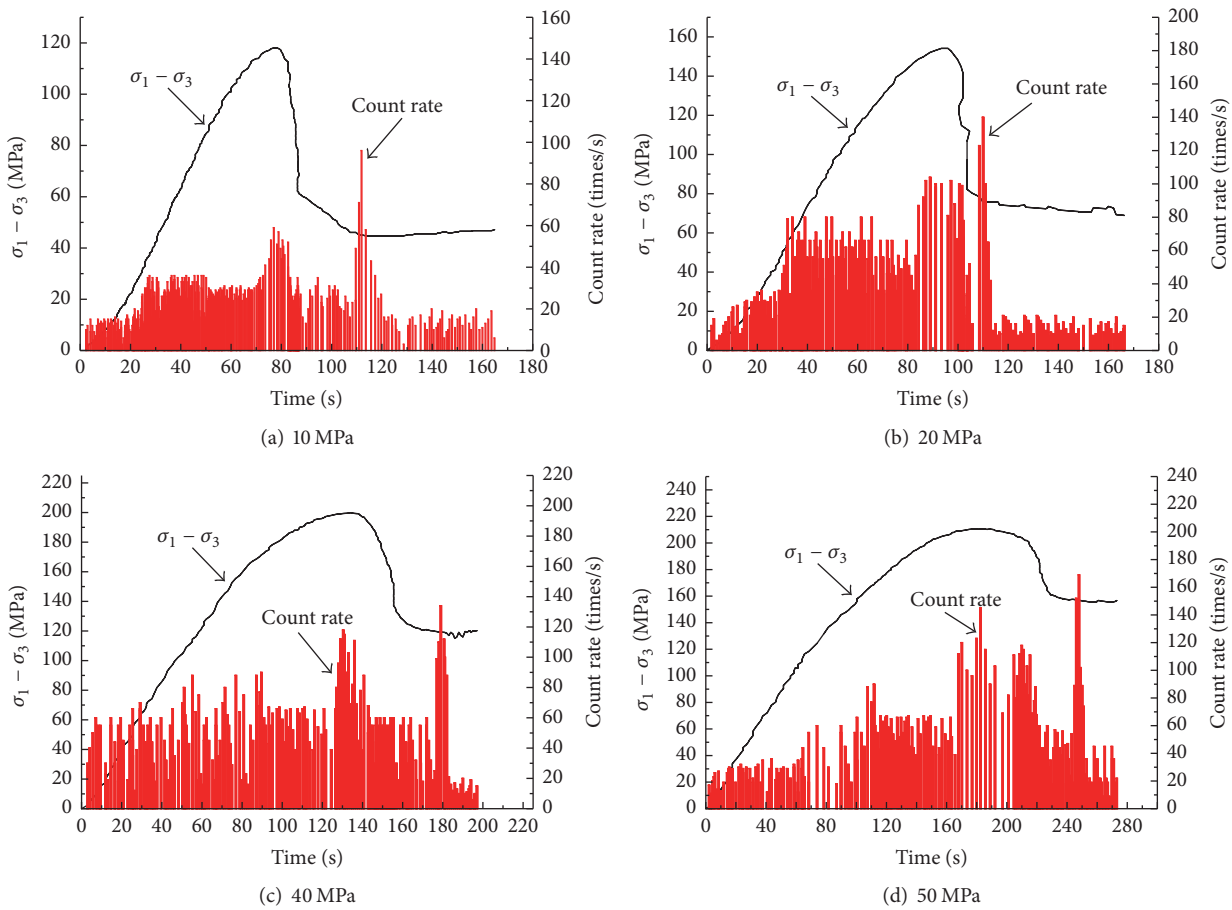

Figure 3: Curves of axial stress difference and count rate with time in sandstone failure process under various confining pressures in Scheme I.

of samples, prolongs the crack propagation process, delays the breaking moment, and increases the AE ringing count rate, which can provide the basis for identifying the failure point.

4.2. AE Characteristics of Samples under Unloading Conditions. Figures 4 and 5 show the curves of axial stress difference and count rate with time in sandstone failure process under various confining pressures in Scheme II and Scheme III, respectively. In Scheme II, as shown in Figure 4(a), the ringing rate gradually increases before unloading point. The results show that there exists an apparent turning point at the unloading point in the stress-strain curves and there is a sudden increase in the count rate. The sandstone sample is suddenly destroyed 10 s after unloading point, and the count rate comes to the maximum value of 131 times/s at 74.9 s. As shown in Table 2, the count rate at the peak increases from 131 times/s to 296 times/s with the confining pressure increasing from 10 MPa to 50 MPa, indicating that the samples are destroyed more fiercely with the confining pressure increasing. As shown in Figure 4(b), the count rate-time curve emerges with a quiet period of 30 s before unloading. There are no new cracks to initiate in the samples, so they cannot be regarded as the precursor information of sample failure. When the sample begins to be unloaded, the count rate has a sudden increase, indicating that the new cracks occur in the samples. The count rate continues to increase with unloading until the axial stress difference at the peak rises to 148.03 MPa.

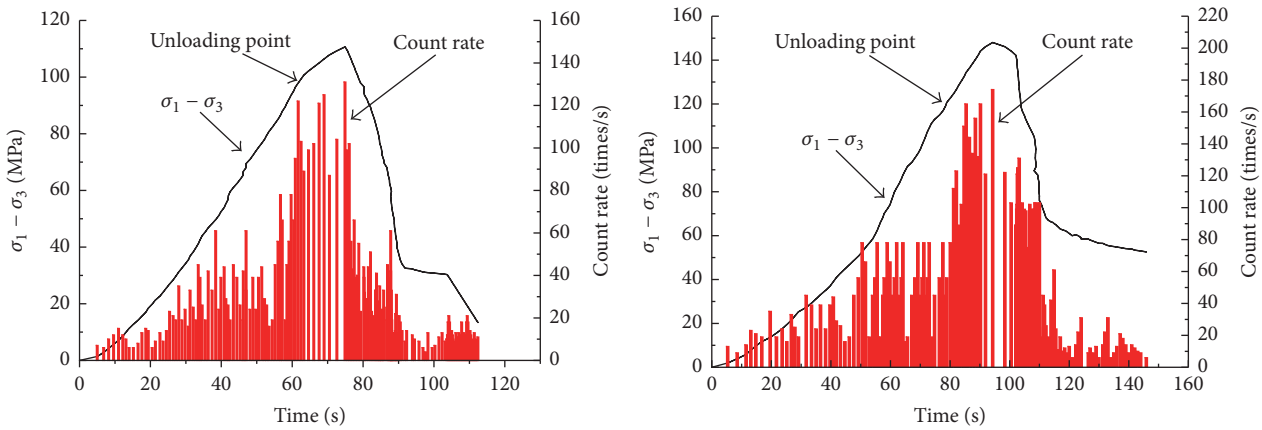

(a) 10 MPa (b) 20 MPa

Figure 4: Curves of axial stress difference and count rate with time in sandstone failure process under various confining pressures in Scheme II.

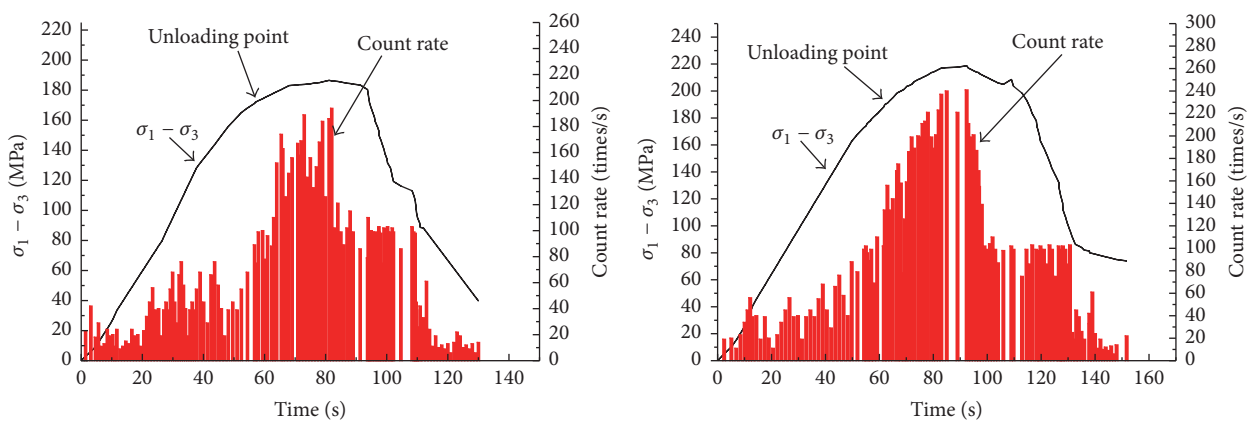

(a) 30 MPa (b) 40 MPa

Figure 5: Curves of axial stress difference and count rate with time in sandstone failure process under various confining pressures in Scheme III.

The count rate of Scheme III has the same change rules as that of Scheme II. Unlike the Scheme I, there are no obvious precursory characteristics before failure in Schemes II and III, and the count rate reaches the maximum at failure.

5. Acoustic Emission Failure Precursors of Sandstone under Different Loading and Unloading Paths

5.1. The Calculation of Fractal Dimension. To further investigate the failure precursors of sandstone samples under different stress paths, it is necessary to quantify the characteristics of the acoustic emission during the whole failure process [19–22]. The acoustic emission count rate has a fractal feature in the time series analysis. The delay-coordinate method is adopted to reconstruct the space phase and fully reveal the information contained in the time series. Assuming that the relationship between dimension m of delay-coordinate and dimension d of the sequence is $m \geq 2d + 1$, the calculation process based on the G- P algorithm is as follows: the strength sequence of acoustic emission of one sample in the process of the tests is studied, which corresponds to a sequence set with a capacity of n.

$$X = \{x_1, x_2, \ldots, x_n\}. \tag{1}$$

Taking m paratactic numbers in the sequence as the first vector in m-dimensional space,

$$Y_1 = \{x_1, x_2, \ldots, x_m\}. \tag{2}$$

Moving the m paratactic numbers back for one position and taking another m paratactic number in the sequence as the second vector in m-dimensional space,

$$Y_2 = \{x_2, x_3, \ldots, x_{m+1}\}. \tag{3}$$

Then, $N = n - m + 1$ vectors are formed. According to the Takens principle, the correlation dimension of the sequence is calculated. The correlation dimension is the cumulative

Table 2: Count rate of sandstone sample under various confining pressures in Schemes II and III.

Stress path	Confining pressure/MPa	Axial stress difference at the peak/MPa	Time at the peak/s	Count rate at the peak/(times/s)	Maximum count rate/(times/s)
Scheme II	10	110.67	74.9	131	131
	20	148.03	94.3	174	174
	40	186.03	122.6	211	211
	50	207.39	146.9	296	296
Scheme III	10	109.57	57.13	112	112
	20	152.31	72.3	159	159
	40	186.49	81.12	194	194
	50	218.74	92.4	241	241

distribution function $W(r)$, that is, the probability that the distance of two points is less than r in the space.

$$W(r) = \frac{1}{N^2} \cdot \sum_{i,j}^{N} u\left(r - \left|Y_i - Y_j\right|\right), \tag{4}$$

where u is the Heaviside function.

$$u\left(r - \left|Y_i - Y_j\right|\right) = \begin{cases} 1 & \left(u\left(r - \left|Y_i - Y_j\right|\right) \geq 0\right) \\ 0 & \left(u\left(r - \left|Y_i - Y_j\right|\right) < 0\right). \end{cases} \tag{5}$$

$|Y_i - Y_j|$ is the distance between Y_i and Y_j, and r is the measurement scale. The slope can be obtained based on of straight-line fitting of data point $(\lg W(r), \lg r)$:

$$D(m) = \frac{\lg W(r)}{\lg r}. \tag{6}$$

This is the fractal feature of the strength sequence of acoustic emission within the measurement scale. The line slope D gradually converges to a stable value with the dimension m increasing; otherwise, the sequence set is a random sequence. When the strength sequence of acoustic emission is constant, the smaller the fractal dimensions, the narrower the distribution of strength in the sequence, and the strength values are close.

5.2. Variation of Fractal Dimension with the Stress Ratio. Programs are made to calculate the fractal dimensions of acoustic emission of sandstone samples during the failure process. Rock samples usually fail as the stress is loaded to the peak value of compressive strength. Thus, using the peak stress difference as a baseline, the stress ratio is defined as the ratio of axial stress difference and peak stress difference. The maximum of the stress ratio is 1.

Table 3 gives the fractal values of AE of sandstone samples under different stress ratios, and Figure 6 shows the curves of the fractal values. As shown in Figures 6(a) and 6(b), when the stress ratio ranges from 0.2 to 0.4, the sandstone samples are at the stage of transferring from initial compression to elastic deformation. Under the influence of confining pressure, the growth rate of fractal values is slow, which even shows a decrease. When the stress ratio ranges from 0.4 to 0.8, the cracks in the samples under conventional triaxial loading tests propagate slowly, and the fractal values first increase and then decrease. The samples under unloading conditions enter into the plastic deformation stage from the elastic deformation stage; thus, the crack growth rates increase obviously and the fractal values first decrease and then increase. When the stress ratio ranges from 0.8 to 1.0, the stress of the samples approaches the peak value and the cracks in the samples expand and communicate into a shear band. The formation of the shear band induces the brittle failure of the samples, and the fractal values under different stress paths decrease rapidly. The acoustic emission at this stage can be used to investigate the failure precursors of the samples under different stress paths. By contrast, the decreasing rate of the fractal values of Scheme II is the highest, followed by that of Scheme III. The decreasing rate of Scheme I is the lowest.

When the confining pressure increases, as shown in Figures 6(c) and 6(d), the fractal values of the sandstone samples show different changing tendencies. As the stress ratio ranges from 0.4 to 0.8, the initiation, propagation, and coalescence of cracks in the sandstone samples slow down when subjected to the high confining pressure. The variation trend of the fractal values of the samples under unloading conditions is similar to that under conventional triaxial loading conditions; that is, they first increase and then decrease. When the stress ratio ranges from 0.8 to 1.0, the increase in the confining pressure not only reduces the difference in the AE characteristics between the different stress ratios, but also changes the decreasing regularity of the fractal values of the samples before failure. Therefore, the relationship between AE characteristics and stress ratios is not obvious when the confining pressure is higher (40 MPa or 50 MPa).

5.3. Variation of Fractal Dimension with the Time Ratio. Taking the failure time as a benchmark, the time ratio is designed as the loading time and the failure time. The maximum of the time ratio is 1. Table 4 gives the fractal values of AE for sandstone samples under different time ratios, and Figure 7 shows the curves of the fractal values. According to Figures 7(a) and 7(b), it is found that when the time ratio ranges from 0.4 to 0.8, the fractal values of the sample under different stress paths first decrease and then increase. The variation trend of the AE characteristics is not obvious when the time ratio is greater than 0.8. As shown in Figures 7(c) and 7(d), the fractal values of sandstone samples in Scheme I under

Table 3: Fractal values of AE of samples under different stress ratios.

Stress ratio	Scheme I				Scheme II				Scheme III			
	10 MPa	20 MPa	40 MPa	50 MPa	10 MPa	20 MPa	40 MPa	50 MPa	10 MPa	20 MPa	40 MPa	50 MPa
0.2	1.51	0.90	1.41	1.31	1.21	0.67	0.67	1.26	0.69	0.73	0.83	0.56
0.4	1.34	0.96	1.21	1.23	1.26	0.69	0.69	0.98	0.63	0.62	0.92	0.98
0.6	1.38	1.01	1.29	1.34	1.03	0.61	0.63	1.19	0.51	0.48	0.90	1.12
0.8	1.12	0.79	1.23	1.31	1.19	0.85	0.85	1.16	0.72	0.54	0.83	1.08
1.0	0.91	0.69	1.51	1.40	0.62	0.30	0.31	1.20	0.31	0.41	0.97	0.98

Table 4: Fractal values of AE of samples under different time ratios.

Time ratio	Scheme I				Scheme II				Scheme III			
	10 MPa	20 MPa	40 MPa	50 MPa	10 MPa	20 MPa	40 MPa	50 MPa	10 MPa	20 MPa	40 MPa	50 MPa
0.2	1.33	0.96	1.34	1.34	1.21	0.71	0.69	1.10	0.79	0.69	0.82	0.58
0.4	1.26	1.10	1.36	1.30	1.24	0.66	0.69	1.21	0.56	0.51	0.95	1.11
0.6	1.16	0.78	1.39	1.41	1.13	0.16	0.66	1.06	0.51	0.43	0.87	1.02
0.8	1.19	0.76	1.32	1.41	1.34	0.26	0.86	0.78	0.64	0.64	0.91	0.95
1.0	1.24	0.51	1.34	1.40	1.12	0.69	0.30	0.31	0.66	0.11	0.36	0.08

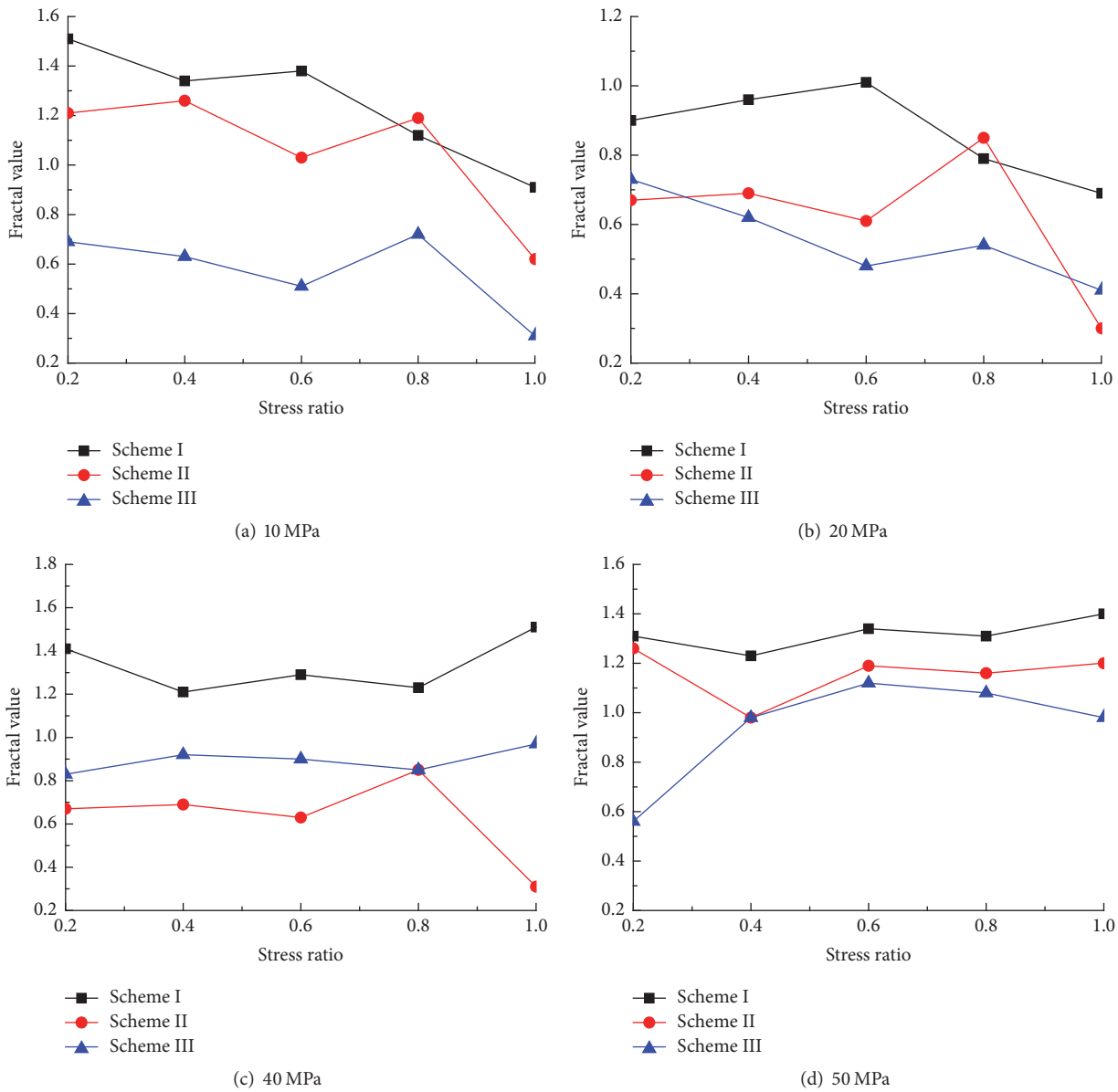

Figure 6: Fractal values of AE of sandstone samples under different stress paths (stress ratio).

different time ratios show little change. When the time ratio is greater than 0.8, the fractal values of sandstone samples under unloading paths are rapidly reduced, which indicates that the fractal value changing with the time ratio can be used to predict rock failure at higher confining pressures.

The failure of rock mass is an energy dissipation process, and the fractal law of the laboratory sample is united with that of engineering rock mass. Theoretically, the fractal dimension of acoustic emission is the efficacious index that evaluates the rock mass stability, and the lowest level of the fractal dimension means that the rock engineering disaster is a strong possibility. In engineering applications, the microseismic (MS) monitoring system can be established to carry out the real time monitoring to the deformation and failure of rock mass, and the AE signals obtained from the MS monitoring can be used to predict the instability of rock mass. In addition, the critical value of the AE signals needs to be studied further.

6. Conclusion

In this paper, a series of triaxial loading and unloading tests of sandstone samples were carried out under different stress conditions. The AE characteristics of sandstone samples under different stress paths were investigated. Based on the fractal theory, the influence of loading and unloading paths on AE characteristics was quantified. The results drawn from the experiments can provide a theoretical basis for assessing the stress-induced stability of hard rock.

(1) The AE quiet period in Scheme I becomes much more obvious with the confining pressure increasing, because the

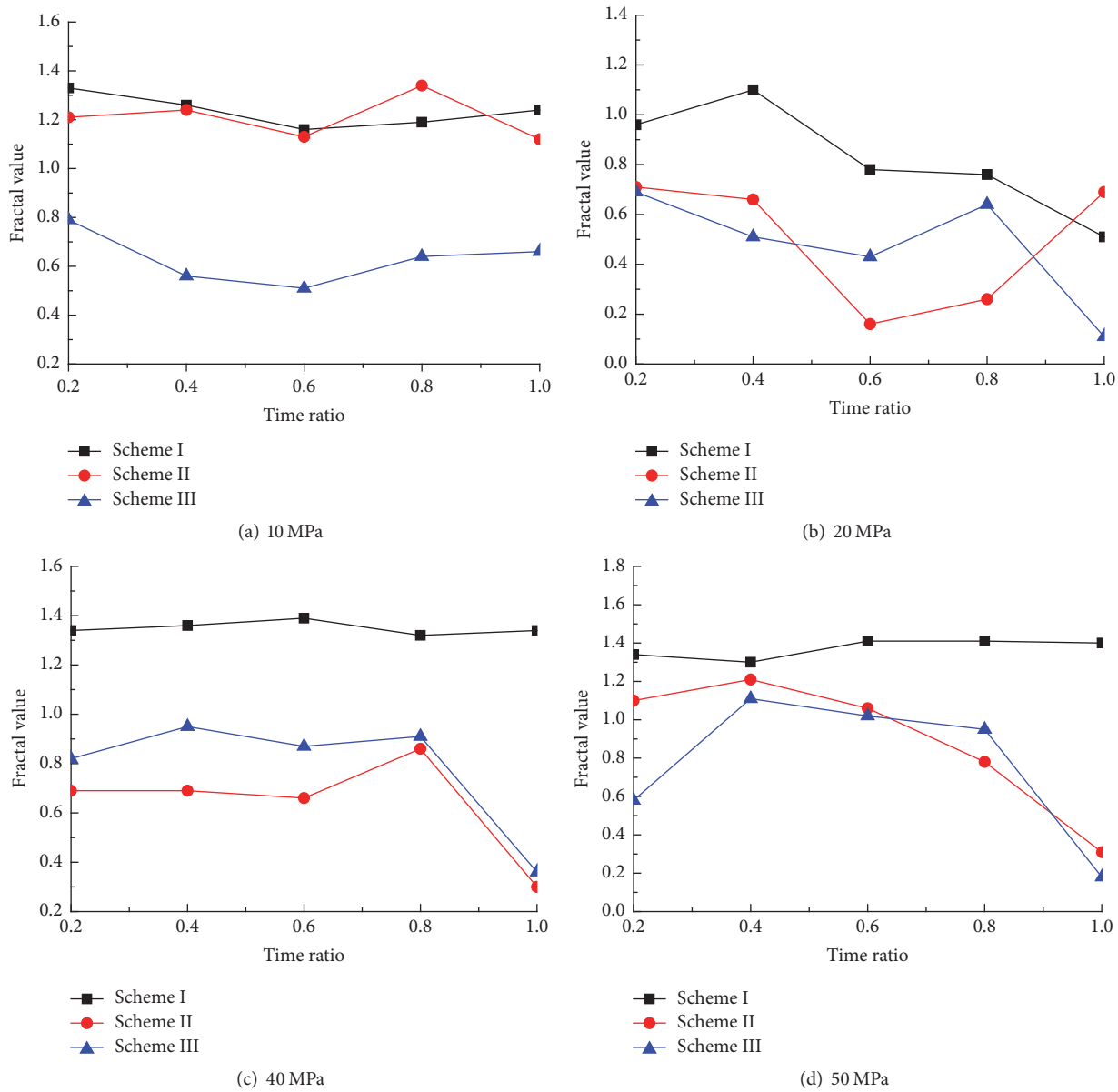

Figure 7: Fractal values of AE of sandstone samples under different stress paths (time ratio).

amount of new cracks is relatively less due to the restriction of higher confining pressure. The time of quiet period lasts from 20 s to 57 s with the confining pressure increasing from 10 MPa to 50 MPa, and the crack propagation process transits from generation oriented to coalescence oriented small cracks. The AE quiet period can be regarded as the precursor information of the sample failure under conventional triaxial compression. The maximum ringing count rate appears after peak instead of peak positions, which also rises with the confining pressure increasing. The reason is that the samples have larger load bearing capacity at peak positions due to the confining pressure constraints, and the obvious friction slip of broken blocks takes place only when the stress falls to the residual stress.

(2) The ringing count rate of Scheme III has the same change rules as that of Scheme II. Unlike Scheme I, there are no obvious precursory characteristics before failure in Schemes II and III, and the ringing count rate reaches the maximum at the peak point.

(3) When the stress ratio ranged from 0.8 to 1.0 under lower confining pressure, the formation of a shear band induced the brittle failure of the samples, and the fractal values under different stress paths decreased rapidly. The fractal values of acoustic emission at this stage can be used to investigate the failure precursors of samples under different stress paths. By contrast, the decreasing rate of the fractal values of Scheme II was the highest, followed by that of Scheme III, and the decreasing rate of Scheme I was the

lowest. However, the relationship between AE characteristics and stress ratios was not obvious when the confining pressure was higher (40 MPa or 50 MPa).

(4) When the time ratio was greater than 0.8 under higher confining pressures, the fractal values of sandstone samples under the unloading paths were rapidly reduced, which indicated that the fractal value changing with the time ratio can be used to predict rock failure at higher confining pressures.

Conflicts of Interest

The authors declare that there are no conflicts of interest regarding the publication of this paper.

Acknowledgments

This work was supported by China Postdoctoral Science Foundation (Grant no. 2017M611676), Jiangsu Province Postdoctoral Research Funding Scheme (Grant no. 1701091B), the National Natural Science Foundation of China (Grant no. 41630638), and the National Key Basic Research Program of China ("973" Program) (Grant no. 2015CB057901).

References

[1] D. A. Lockner, J. D. Byerlee, V. Kuksenko, A. Ponomarev, and A. Sidorin, "Quasi-static fault growth and shear fracture energy in granite," *Nature*, vol. 350, no. 6313, pp. 39–42, 1991.

[2] J. F. Shao and R. Khazraei, "A continuum damage mechanics approach for time independent and dependent behaviour of brittle rock," *Mechanics Research Communications*, vol. 23, no. 3, pp. 257–265, 1996.

[3] M. S. Diederichs, "Manuel rocha medal recipient rock fracture and collapse under low confinement conditions," *Rock Mechanics and Rock Engineering*, vol. 36, no. 5, pp. 339–381, 2003.

[4] Y. Fialko, D. Sandwell, D. Agnew, M. Simons, P. Shearer, and B. Minster, "Deformation on nearby faults induced by the 1999 Hector Mine earthquake," *Science*, vol. 297, no. 5588, pp. 1858–1862, 2002.

[5] F. Rojat, V. Labiouse, P. K. Kaiser, and F. Descoeudres, "Brittle rock failure in the steg lateral adit of the lötschberg base tunnel," *Rock Mechanics and Rock Engineering*, vol. 42, no. 2, pp. 341–359, 2009.

[6] V. B. Smirnov, A. V. Ponomarev, and A. D. Zavyalov, "Acoustic structure in rock samples and the seismic process," *Physics of the Solid Earth*, vol. 31, pp. 38–58, 1995.

[7] A. Zang, F. C. Wagner, S. Stanchits, G. Dresen, R. Andresen, and M. A. Haidekker, "Source analysis of acoustic emissions in Aue granite cores under symmetric and asymmetric compressive loads," *Geophysical Journal International*, vol. 135, no. 3, pp. 1113–1130, 1998.

[8] M. Cai, P. K. Kaiser, and C. D. Martin, "Quantification of rock mass damage in underground excavations from microseismic event monitoring," *International Journal of Rock Mechanics and Mining Sciences*, vol. 38, no. 8, pp. 1135–1145, 2001.

[9] S. Colombo, I. G. Main, and M. C. Forde, "Assessing damage of reinforced concrete beam using 'b-value' analysis of acoustic emission signals," *Journal of Materials in Civil Engineering*, vol. 15, no. 3, pp. 280–286, 2003.

[10] A. Schiavi, G. Niccolini, P. Tarizzo, A. Carpinteri, G. Lacidogna, and A. Manuello, "Acoustic emissions at high and low frequencies during compression tests in brittle materials," *Strain Journal*, vol. 47, no. 2, pp. 105–110, 2011.

[11] Q. S. Liu, J. Xu, X. W. Liu, J. Jiang, and B. Liu, "The role of flaws on crack growth in rock-like material assessed by AE technique," *International Journal of Fracture*, vol. 193, no. 2, pp. 99–115, 2015.

[12] A. Chmel and I. Shcherbakov, "A comparative acoustic emission study of compression and impact fracture in granite," *International Journal of Rock Mechanics and Mining Sciences*, vol. 64, pp. 56–59, 2013.

[13] K. Baddari, A. D. Frolov, V. Tourtchine, and F. Rahmoune, "An integrated study of the dynamics of electromagnetic and acoustic regimes during failure of complex macrosystems using rock blocks," *Rock Mechanics and Rock Engineering*, vol. 44, no. 3, pp. 269–280, 2011.

[14] B. D. Thompson, R. P. Young, and D. A. Lockner, "Fracture in Westerly granite under AE feedback and constant strain rate loading: nucleation, quasi-static propagation, and the transition to unstable fracture propagation," *Pure and Applied Geophysics*, vol. 163, no. 5-6, pp. 995–1019, 2006.

[15] S. C. Xu, X. T. Feng, and B. R. Chen, "Acoustic emission characteristics and mechanical behavior of skarn under uniaxial cyclic loading and unloading," *Controlling Seismic Hazard and Sustainable Development of Deep Mines*, vol. 1, 2009.

[16] S. Zhang, J. Liu, and C. Shi, "Study on precursory characteristics of rock failure based on acoustic emission experiment," *Metal Mine*, 2008.

[17] J.-L. Wang and Z.-J. Li, "Extreme-point symmetric mode decomposition method for data analysis," *Advances in Adaptive Data Analysis (AADA)*, vol. 5, no. 3, pp. 135–170, 2013.

[18] L. A. M. Camones, E. do Amaral Vargas, R. P. de Figueiredo, and R. Q. Velloso, "Application of the discrete element method for modeling of rock crack propagation and coalescence in the step-path failure mechanism," *Engineering Geology*, vol. 153, no. 2, pp. 80–94, 2013.

[19] S. Yuyama, T. Okamoto, M. Shigeishi, and M. Ohtsu, "Quantitative evaluation and visualization of cracking process in reinforced concrete by a moment tensor analysis of acoustic emission," *Materials Evaluation*, vol. 53, no. 6, pp. 751-752, 1995.

[20] T. Shiotani, M. Ohtsu, and K. Ikeda, "Detection and evaluation of AE waves due to rock deformation," *Construction and Building Materials*, vol. 15, no. 5-6, pp. 235–246, 2001.

[21] D. G. Aggelis, S. Verbruggen, E. Tsangouri, T. Tysmans, and D. Van Hemelrijck, "Characterization of mechanical performance of concrete beams with external reinforcement by acoustic emission and digital image correlation," *Construction and Building Materials*, vol. 47, pp. 1037–1045, 2013.

[22] G. Ma and H. Li, "Acoustic emission monitoring and damage assessment of FRP-strengthened reinforced concrete columns under cyclic loading," *Construction and Building Materials*, vol. 144, pp. 86–98, 2017.